Environ. Sci. Technol. **1997**, *31*, 105−113

Estimating Sorption Rates of Hydrophobic Organic Compounds in Iron Oxide- and Aluminosilicate Clay-Coated Aquifer Sands

BRITT A. HOLMÉN† AND PHILIP M. GSCHWEND*

Ralph M. Parsons Laboratory, 48-415, Massachusetts Institute of Technology, Cambridge, Massachusetts 02139

We hypothesized that retarded diffusion in coatings controls the rate of sorption of hydrophobic organic compounds (HOCs) on quartzitic aquifer sands. Microscopic examination of three sands was used to quantify the coating thicknesses. With measures of the coatings' organic contents and porosities, we predicted the relative sorption rates for (a) multiple HOCs on one sand and (b) one HOC with three sands. The predicted relative rates and equilibrium coefficients were assessed using observations of HOC transport through short sand columns operated at varying flow rates. We found that the column K_d values were always much less than predicted from $K_{oc}f_{oc}$ or observed in batch tests. This suggests that diagenetically produced sorbents may include organic matter that is completely inaccessible for HOC sorption; procedures that disaggregate these sands could expose organic matter that does not sorb HOCs in the environment. Second, by modifying our retarded diffusion expectations with the inferred fraction of available organic carbon, f_{avail}, all observed sorption rates were consistent (within a factor of 4) with $k_r \approx 0.001D_{aq}/\delta^2(1 + r_{sw}^{coat}K_{oc}f_{oc}^{coat}f_{avail})$, where k_r is the desorption rate constant, D_{aq} is the HOC's aqueous diffusivity, δ is the coating thickness, r_{sw}^{coat} is the ratio of solids-to-water in the coatings, f_{oc}^{coat} is the organic carbon content of the coating solids, and all other factors affecting sorption rates (e.g., tortuosity) were set equal to 0.001. Since oxide coatings are ubiquitous in aquifer sands, the model described here should have wide applicability.

Introduction

Sandy aquifers are important sources of groundwater. Anthropogenic contamination of these resources and the need to remediate them in a cost-effective manner warrant understanding the processes that affect subsurface contaminant transport in such aquifers. For hydrophobic organic compounds (HOCs), sorption is a critical process governing the fate of these chemicals in groundwater. Recent field and laboratory evidence has demonstrated that subsurface HOC sorption is often not well-described as an equilibrium process (*1, 2*). Thus, quantifying sorption kinetics is key to generating accurate models of HOC transport and transformation in sandy aquifers and designing effective cleanup techniques.

Numerous studies have examined the rate of sorption to natural solids and concluded that diffusive transport limits the rate of solute uptake and release (*3*−*7*). Such research has shown that mass transfer factors such as particle diameter, sorbate diffusivity, and sorbent tortuosity are critical parameters for predicting HOC sorption kinetics (*4, 5, 8, 9*). However, many questions remain concerning the mechanism and, thus, the rate-limiting step. Three potential diffusive mass-transfer bottlenecks exist: (1) diffusion of sorbate across an aqueous boundary layer on the exterior of aquifer sand particles; (2) pore or surface diffusion among the aggregated minerals that constitute natural particles; or (3) diffusion within the ultimate, microscopic-scale, sorbent phase (e.g., within the natural organic matter, OM).

Boundary layers on the exteriors of aquifer solids cannot exceed the pore scale in thickness. Therefore, diffusion across this external water medium is generally considered to be fast and is justifiably neglected (e.g., time scale < (pore scale^2/aqueous diffusivity) $\sim$ [$(10^{-2}$ cm$)^2/10^{-5}$ cm^2/s] = 10 s).

Diffusion rates within natural organic matter [commonly presumed to be the predominant sorbent medium for HOCs interacting with water−wet natural solids containing some minimal OM (*10*−*12*)] should be consistent with diffusion in synthetic organic polymers (e.g., refs 13−17). We expect that intraorganic matter diffusion should be a function of OM composition, swelling, cross-linking, and dimension. Brusseau and Rao (*18*) suggest that intraorganic matter diffusion is the rate-limiting HOC sorption regime in nonaggregated sorbents. We examine this mechanism for our aggregated sorbents and rule it out (see Discussion).

As the aquifer sands studied here consist of aggregated solid fines coating larger framework grains, our discussion focuses on the third rate-limiting process, often referred to as "retarded radial diffusion". Within natural sorbent *aggregates*, retarded radial diffusion should be a strong function of the diffusive path length as well as the abundance and distribution of OM sorption sites (*4, 5, 7, 9, 19*). To date, research has generally employed the particle grain radius as the appropriate diffusive length scale (e.g., *4, 6, 7, 9, 20, 21*). Since silty sorbents are typically aggregates of fine particles from exterior to interior (*9, 20*), this length scale (or a weighted mix of lengths for widely varying particle size distributions) appears suitable for cases involving silty sediments and soils. However, this length scale choice is inconsistent with reports in which (1) best-fit particle radii varied for different compounds in a single sorbent (*19*), (2) desorption rate was insensitive to particle radius (*21*), and (3) early- versus late-desorption time courses required different best-fit diffusion lengths (*7*). Furthermore, some studies have not observed the expected increase in sorption rate after pulverizing the sorbent (*6*), although other studies have seen such behavior (*4*).

For many aquifer sands, we suggest that OM-rich iron oxyhydroxide and aluminosilicate clay coatings, located at the exteriors of the framework sand grains, are the principle HOC sorption media. Iron oxide coatings are prominent in many aquifer materials. For example, Stauffer (*22*) reported petrographic analyses for six aquifer materials, and all six aquifer solids had significant iron oxide coatings on quartz and feldspar grains. MacIntyre et al. (*23*) also reported goethite and lepidocrocite coatings on quartz grains from alluvial terrace aquifer material from Columbus, MI. Other aquifer sorbents with appreciable iron oxide coatings include Borden (*24*), Cape Cod (*25*), the New Jersey Pine Barrens (*26*), Lula, OK, and Tampa, FL (*1*). Such iron oxide appears to "cement" various other fines (such as the aluminosilicate clays and macromolecular natural OM) together as coatings on, and matrix between, larger sand grains (*26*).

* Corresponding author phone: (617)253-1638; fax: (617) 253-7395.

† Present address: Department of Land, Air and Water Resources, University of California, Davis, CA 95616.

S0013-936X(96)00169-1 CCC: $14.00

The association of natural organic matter with iron- and aluminum-bearing minerals has been attributed to sorption of negatively charged OM to positively charged oxide mineral surfaces under natural surface and groundwater conditions (*27*−*29*). Soil scientists have noted the association of humic acids with iron oxides (*30*−*32*) and the ability of organic matter to inhibit iron oxide crystallization (*33*−*35*). This intimate association of OM with iron and aluminum oxides (including clay edges) and the observation that HOC sorption occurs via nonspecific interactions with sorbent organic matter (*12, 36*−*38*) leads us to propose that HOC sorption kinetics for such aquifer sands can be described as a mass transfer problem in which sorbates must diffuse to and from a single type of sorption site (natural OM), distributed within the fine-grained aggregates that coat or lie between the larger framework aquifer grains.

Theory for HOC Transport Through Coated Sands. Transport of HOCs through coated sands can be described by coupling the advection−dispersion transport equation for porous media with a grain-scale mass transfer model. Appropriate models have previously been developed for gas−solid chromatography because the immobile stationary phases consist of porous packings with impermeable core regions (*39*). This conceptualization is appropriate for many aquifer sands since the primary mineral grains are rimmed by porous, high f_{oc}, iron oxide/clay coatings. Also, we do not expect the interiors of mineral grains to be important sites of sorption of HOCs due to the low f_{oc} in these regions of the sands. Note that we assume mass transfer to the sites of accessible OM within the coatings is limiting transport, but sorptive equilibrium prevails at each submicron-scale OM location.

The solution to such a porous coating diffusion model (e.g., ref 39) involves an effective diffusivity parameter that incorporates sorbate diffusivity, intraaggregate porosity, constrictivity, tortuosity, and intraparticle retardation. Some of these terms are difficult to estimate *a priori*. The diffusive mass transfer process can however be approximated by a first-order mass-transfer model, and the rate coefficient can be deduced by equating second moment expressions (*40*). This simplification allows one to quantify, via the method of moments, an equivalent reverse sorption rate constant, k_r, without explicitly quantifying sorbent geometry factors such as constrictivity and tortuosity. As a result, the coated sand desorption rate, k_r (s^{-1}), is related to the diffusion model parameters by

$$k_r \approx \frac{D_{aq}}{\delta^2 R_{coat}} G \qquad (1)$$

where D_{aq} is the sorbate aqueous diffusion coefficient (cm^2/s), δ is the coating thickness (cm), R_{coat} describes the intracoating retardation factor (−), and G is a factor that incorporates all the geometric factors of the sorbent, including porosity, tortuosity, constrictivity, and particle geometry (e.g., ratio of coating thickness to particle radius, particle shape) as well as system variables (closed vs open system, solid-to-water ratio) (*20, 41*).

For a single sorbent, the G and δ factors in eq 1 will be approximately constant for sorbates of similar size. Thus, we examined the rate of sorption, k_r, for three polycyclic aromatic hydrocarbons (naphthalene, acenaphthene, and phenanthrene) in a single sand column to test whether or not k_r varied with $[R_{coat}]^{-1}$ as expected based on eq 1. Furthermore, assuming diagenetically produced iron oxide/clay coating geometry factors (G) are similar among aquifer sands, we also evaluated the hypothesis that k_r varies with $[\delta^2 R_{coat}]^{-1}$ by measuring k_r for a single sorbate (acenaphthene) and three well-characterized aquifer sands.

Methods

Sorbent Characterization. The Pine Barrens, NJ (PB), sand is a Miocene beach deposit and was previously characterized (*26*). The Georgetown, SC (GT), sand is also an iron oxide- and kaolinite-coated Atlantic Coastal Plain beach deposit, but has a different texture and mineralogy. The Aberjona, MA (AJ), sand is a Pleistocene glacial outwash deposit. The bulk sands were dried at 70 °C and then sieved through 1000, 250, 105, and 53 μm screens to give five size fractions. These fractions were further characterized for organic carbon content, mineralogical composition, and iron content. A second bulk sample was sonicated in distilled water for 30 min prior to wet sieving through the four screens. A Perkin-Elmer Model 2400 CHN analyzer was used for fraction organic carbon (f_{oc}) determination after the larger sieve fractions were ground with a mortar and pestle. Mineralogy and sediment texture were characterized using a Cambridge Stereoscan 240 scanning electron microscope (SEM) equipped with an energy dispersive X-ray spectrometer (Link Analytical). Thin sections of the dry sand fractions were prepared by embedding the sand in low-viscosity Spurrs epoxy and were carbon-coated prior to SEM analysis. Aqueous suspensions of the <53 μm wet-sieved size fraction were air-dried on glass slides for X-ray diffraction (XRD) analysis. The clay-sized fraction (<2 μm) was separated from the bulk sand by standard sedimentation techniques for further XRD characterization. Pore size distribution was determined by Porous Materials Inc. (Ithaca, NY) using mercury intrusion on 2−3 g samples of three fractions (bulk, 250−1000 μm, sonicated 250−1000 μm) for each aquifer material. Pore diameters were calculated using the Washburn equation (*42*) for pressures up to 60 000 psi (approximately 3.5 nm) assuming cylindrical pores, a contact angle of 140°, and a surface tension of 480 dyn/cm. Selected size fractions were analyzed for total iron (*43*), Ti(III)−citrate−EDTA−bicarbonate (TiCEB)-extractable iron (*44*) and oxalate-extractable iron (*45*) by inductively coupled plasma (ICP) analysis of sediment digestates and extracts.

Solutions and Chemicals. Acenaphthene, naphthalene, and phenanthrene solutions were made up in buffer from the solid PAH and were magnetically mixed for at least 1 week prior to use. Sorbate properties were based on data of Miller et al. (*46*). K_{oc} was calculated from Karickhoff's (*47*) regression for PAH sorption to soils: $\log K_{oc} = 0.989 \log K_{ow} - 0.346$. Distilled water was 0.2 μm filtered prior to adding sodium acetate and glacial acetic acid (final concentrations of 10^{-4} M) to buffer the pH near the ambient groundwater values of 4.8 for Pine Barrens, 5.2 for Georgetown, and 5.8 for Aberjona. The buffer also contained mercuric chloride at 10 mg/L to limit biological activity.

Column Experiments. Sorption experiments were conducted with the 250−1000 μm Pine Barrens sand size fraction and with the bulk Georgetown and Aberjona sands. These experiments were conducted as short-column, short pulse-input experiments at a range of pore velocities (see 43). The columns (~7 cm long and 22 mm i.d.) were mirror-finished stainless steel tubing (Alltech Associates; Deerfield, IL) fitted with low-dead-volume high-pressure liquid chromatography (HPLC) end caps with 2 μm stainless steel frits. A stainless steel buffer reservoir was sampled using a Waters Model 501 HPLC pump, which pumped buffer to an injection valve located below the column. The injection port enabled 200 and 500 μL pulse injections of the PAH solution of interest to be fed into the column inlet. Input solution concentrations for sorbates were 110, 19, and 4.5 μM for naphthalene, acenaphthene, and phenanthrene, respectively, and 10^{-4} and 0.02 M for the nitrate and acetone conservative tracers. Column effluent was continuously monitored with either a Waters Model 484 absorbance detector (naphthalene, nitrate, acetone, and acenaphthene) or a Waters Model 470 fluorescence detector (phenanthrene). The detector was located as close to the column outlet as possible (approximately 2.5

cm and 5 μL) in order to minimize apparatus dispersion. After passing through the detector cell, the column effluent was collected in tared flasks to monitor flow rate gravimetrically. Mass balances were carried out on five column experiments by analyzing the effluent concentration via fluorescence. Recoveries were between 88 and 110% for all three PAH compounds. Column experiments were carried out over a range of pore velocities (0.5−115 cm/h) in order to evaluate sorption parameters from the dependency of the first two moments of the pulse-input elution curves on column flow rate (see Schneider and Smith (*39*)). To facilitate data processing, the output of the detectors was sent to a data acquisition system, and the moments of the elution pulses were calculated using the trapezoidal rule for integrations.

Data Analysis. The method of moments was used to analyze our sand column elution curves. Using boundary conditions that also apply to our experiments, Schneider (*39*) solved the coupled diffusion equations in the Laplace domain and reported the time-moment formulas for the first absolute moment (μ_1') and second central moment (μ_2). By analogy with the moment expressions of Valocchi (*48*) for a single-site first-order sorption model, Schneider's moment expressions were reduced to

$$\mu_1' = \frac{L}{v}R_f + \frac{t_0}{2} \tag{2}$$

$$\mu_2 = \frac{2L\alpha\, R_f^2}{v^2} + \frac{2L[R_f - 1]}{vk_r} + \frac{t_0^2}{12} \tag{3}$$

where L is the column length (cm), v is the column pore water velocity (cm/s), R_f is the column retardation factor, t_0 is the pulse duration (s), α is the dispersivity (cm) (we assumed dispersion coefficient (cm^2/s) = αv), and k_r is the first-order desorption rate coefficient (s^{-1}).

The model parameters L, R_f, α, and k_r were quantified by curve-fitting the experimental moments to eqs 2 and 3 as functions of inverse velocity. One standard deviation error for each model parameter was calculated using propagation-of-error techniques based on the standard errors (SE) obtained from the curve-fits. The breakthrough curves (BTCs) for each individual compound were truncated at the same number of pore volumes to minimize artifacts due to detector noise and drift. Truncation bias was quantified using simulated breakthrough curves generated with the computer program CXTFIT (*49*) operated as a single-site model for a range of pore velocities (0.5−20 cm/h). We found the truncation bias in the rate constant (k_r) to be greatest for the acenaphthene-PB experiments (up to 120%) and attribute this bias to truncation at a pore volume less than 2 times the value of R_f for this sorbate−sorbent pair. Generally, the conclusions discussed below are not affected by a factor of 2 level of accuracy.

Estimating Sorption Rate Coefficients for Coated Aquifer Sands. Previous studies (*4*, *5*, *8*, *9*) have had varying degrees of success in matching measured and predicted effective diffusivities, a fact that highlights our incomplete grasp of the sorption mechanism. For the three aquifer sands we studied, eq 1 suggests that we can estimate *relative* sorption rates if we can assess two parameters for each sand: (1) coating thickness, δ, and (2) coating retardation factor, R_{coat}. The length scale (δ) can be obtained from microscopic examination of the sands, especially in thin section. The latter parameter can be evaluated using the solid-to-water ratio of the coating materials, r_{sw}^{coat}; the coating organic carbon content, f_{oc}^{coat}; and the sorbate's organic-carbon-normalized partition coefficient:

$$R_{coat} = 1 + r_{sw}^{coat} f_{oc}^{coat} K_{oc} \tag{4}$$

In this expression, HOC retardation is assumed to be due to partitioning to OM within the coatings, and the coating partition coefficient, K_d^{coat} (mL/g), was estimated from K_{oc} f_{oc}^{coat}. We estimated f_{oc}^{coat} by assuming that the <53 μm fine fraction we collected after sonicating the bulk sand was representative of the coating materials, and therefore measurement of its organic carbon content would reflect that of the intact coatings/matrix. We also assumed that coating porosities were represented by the difference in pore volumes measured by mercury porosimetry between the unsonicated and the sonicated samples. Since the iron oxyhydroxide and aluminosilicate clay grains in the coating/matrix were about 100−1000 nm in size, we used the integral pore volumes (V_i^{coat}; cm^3/g_{coat}) from 3 to 200 nm in nominal diameter. Thus, r_{sw}^{coat} (g/mL) is given by

$$r_{sw}^{coat} = \left(\int V_{unsonicated}^{coat} - \int V_{sonicated}^{coat}\right)^{-1} \tag{5}$$

By examining the relative magnitudes of the sorption rates deduced from the moment analyses of the BTCs for (a) various HOCs (of known K_{oc}) and a single sand and (b) for one HOC and three sands with measurable r_{sw}^{coat} and f_{oc}^{coat} values, we can test whether our hypothesis of retarded diffusion into sand coatings is consistent with the data.

Results and Discussion

Sand Textures and Coating Properties. The three sands we studied were chiefly composed of quartz with iron oxyhydroxide and aluminosilicate (clay) coatings (Figure 1; Table 1). The three sand textures differed measurably in (1) the abundance of coating/matrix material around/between the framework quartz grains, (2) the abundance of feldspar framework grains, and (3) the porosity of both the coating material and the framework grains. Considering these aquifer materials to be composed of two components (framework grains and fines as coatings and matrix), each sand represents different proportions as well as different compositions of the components. The Pine Barrens sand (Figure 1a) is chiefly quartz grains with goethite and kaolinite coatings, typically about 10 μm in thickness (ranging from 0 to 50 μm). Georgetown sand (Figure 1b) is dominated by fine-grained matrix material (patches up to 200 μm wide) with framework grains (predominantly quartz) occurring as "islands" in the matrix. This sand formed round aggregates about 1 mm in diameter when air-dried. The Aberjona sand (Figure 1c) has coated framework grains (both quartz and feldspar) with typical coating thicknesses of about 20 μm. This sand also has a much higher feldspar (plagioclase and K-feldspar) content than either PB or GT, and many of the feldspar grains are weathered and porous. In addition, no crystalline iron oxide was detected in the <2 μm sample analyzed by X-ray diffraction for AJ, whereas goethite was detected in both PB and GT samples. Based on observations of the sand thin sections (Figure 1), the average diffusion length scales for the three sorbents are about 10, 100, and 20 μm for PB, GT, and AJ, respectively (Table 1). These dimensions are somewhat variable within any one sand and thus should be viewed as no better than a factor of two estimates.

The fine fractions contributed to only a limited portion of each sand's total mass (<53 μm, after sonication: PB, 2%; GT, 12%; AJ, 1%). Although all three bulk sands exhibited quite low organic contents when normalized to the total sand mass (about 0.1% or less), the isolated fines had much greater f_{oc} values (near 1%, Table 1). Likewise, the fine fractions contained a disproportionate share of each sand's readily extractable iron content (PB, 35%; GT, 31%; AJ, 23%). The association between organic matter and iron minerals has previously been noted by Barber et al. (*27*) and led us to suspect that the iron-rich coatings in these sands would be the principle regions of HOC sorption capacity. The porosities of the coatings, deduced by the loss of 3−200 nm pore volume

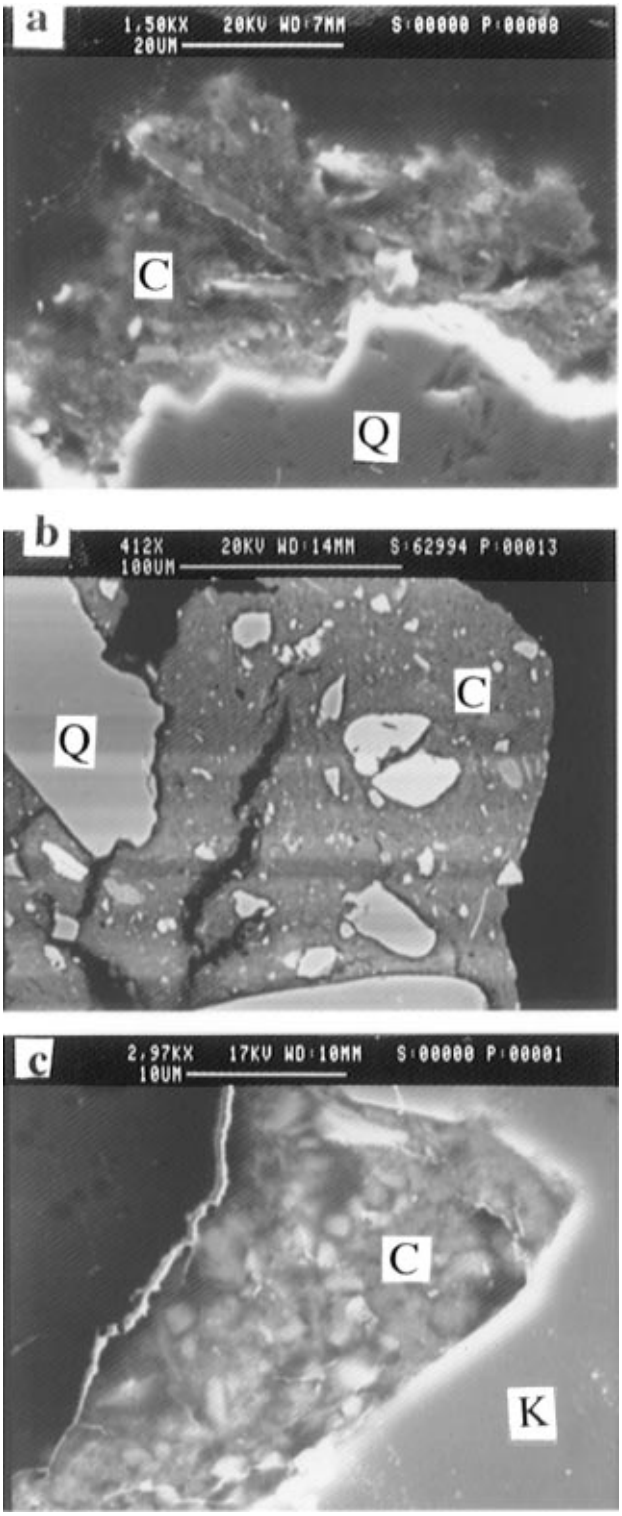

FIGURE 1. (a) Pine Barrens 250−1000 μm fraction SEM micrograph (1500×). Q = quartz, C = coating. Back-scattered electron image of 50 μm thick fine-grained coating composed of Fe, Al, and Si on the edge of quartz grain. (b) Bulk Georgetown sand micrograph (412×) of matrix material that is > 200 μm at widest point and includes many quartz fragments. (c) Bulk Aberjona sand micrograph (2970×) of fine-grained coating in K-feldspar (K) embayment up to 20 μm thick.

after sonicating the sands (Figure 2) were in the range of 0.4−0.5 (Table 1). These porosities suggest solid-to-water ratios in the intact coatings of about 3−4 (Table 1).

Column Experiment Moment Results. The breakthrough curves of the various test compounds transported through the sand columns exhibited the expected relative behaviors. First, for any single column flow rate, compounds of increasing hydrophobicity required more pore volumes to be flushed through the sand columns (Figure 3a). Furthermore, the breakthrough pore volume of any single compound increased as the column flow rate decreased (Figure 3b). Thus, it appears that the times necessary to achieve sorption equilibrium were being bracketed by the column pore fluid contact times (dictated by the range of pore velocities) we used.

Quantitative evaluation of R_f, α, and k_r from the column data was accomplished by fitting the first absolute (μ_1') and second central (μ_2) moments of the conservative tracer and PAH elution curves to eqs 2 and 3. Column properties such as dispersivity and immobile zone retardation were evaluated from the moments of the conservative tracers—nitrate (PB) and acetone (GT and AJ). Generally, the best-fit dispersivities were on the order of the mean grain size, consistent with expectation (*50*), and similar to values reported by other investigators using sand column studies (e.g., refs 51 and 52). Asymmetric acetone elution curves for the GT (Figure 4) and AJ (not shown) columns indicated appreciable immobile water, in contrast to the PB column where the nitrate curves were symmetrical. The presence of immobile water is consistent with relatively longer diffusion path lengths in these sands. These sand-to-sand differences partially reflect the effect of using the GT and AJ bulk sands versus a sieved sand in the PB column. The wider ranges of particle size and pore size distribution in bulk sands relative to the PB sieved sand resulted in much larger dispersivity values for the bulk sand columns (Table 2). Others have noted large dispersivities in aggregated soils (*53*), in sediments of wide particle size distribution (*54*), and for large standard deviations in pore size distributions (*55*).

The moments analyses for the HOCs yielded their transport retardation factors (R_f) and first-order desorption rates (k_r) (Table 2; Figure 5). The R_f values for the three PAHs and the PB sorbent calculated from the first absolute moments (Table 2) increased with increasing hydrophobicity (nap < ace < phen) as one expects for an f_{oc}-controlled sorption process (Figure 5a). The best-fit rate constants (k_r) evaluated from the second central moment fits (Figure 5b and c) imply that the desorption process occurred at rates between about 1 h^{-1} for naphthalene to about 1 day^{-1} for phenanthrene (Table 2). Further, the sand-to-sand variations were not very great (less than a factor of 3). Examining the relative magnitudes of these sorption kinetic results in light of the coating model (eq 1) for the three PAHs and the PB sorbent, one finds good support for our hypothesis that k_r is proportional to $[R_{coat}]^{-1}$ (Table 3). This implies that "tuning" relative sorption rates to what is chiefly an HOC hydrophobicity measure (R_{coat}) can successfully predict these kinetics for a given site.

Evaluation of Intraorganic Matter Diffusion Mechanism. Although the relative rate constants for the three sorbates and the PB sand agree with the coating diffusion model, the alternative mechanism of slow diffusion *within* the sediment natural OM must also be examined. Since natural organic matter is typically thought to consist of macromolecules of nonrepeating structure [e.g., "highly branched polymer chains that form a three-dimensional, randomly oriented network" (*56*)], we believe this sorptive medium should be viewed chiefly as a noncrystalline material. Furthermore, since natural organic matter in soils is found to absorb significant water (*38*), an "elastomer" depiction of OM may be more reasonable than a "glassy" conceptualization.

For the three PAHs we studied, we calculated their diffusion coefficients in natural OM based on the model developed for both elastomer and glassy polymers by Salame (*57*) and recently applied by Carroll et al. (*14*, *15*) (Table 4). For naphthalene, acenaphthene, and phenanthrene, the elastomer polymer diffusivities ranged from about 1×10^{-12} to 3×10^{-14} $cm^2\ s^{-1}$, many orders of magnitude lower than the corresponding aqueous diffusivities. The glassy polymer

TABLE 1. Coating Properties for Three Aquifer Sorbents

property	PB	GT	AJ
	Measured		
bulk sand wt % <53 μm	2.12	12.1	1.19
fines mineralogy[a]	Gt, K	Gt, Gb, K	amFeOx, K, M, Chlr
coating thickness, δ (μm)	10	100	20
coating f_{oc} (%)	0.784 (0.096)	0.648 (0.049)	1.645 (0.024)
bulk sand f_{oc}	0.057	0.109	0.066
pore volume (cm^3/g_{coat}) (for pores ranging from 3 to 200 nm)	0.28	0.27	0.38
	Diffusion Model Parameters (Calculated from Above)		
K_d^{coat} (mL/g) ($=K_{oc}f_{oc}^{coat}$)	7.3 nap 27 ace 120 phen	22	56
n_{coat} (−)	0.41	0.40	0.48
r_{sw}^{coat} (g/mL) (eq 6)	3.6	3.8	2.7
R_{coat} (−) ($= 1 + r_{sw}^{coat}K_{oc}f_{oc}^{coat}$)	27 nap 97 ace 420 phen	83	150
f_{avail} (= column $K_d/K_{oc}f_{oc}$)	0.50	0.05	0.25
R'_{coat} (−) ($= 1 + r_{sw}^{coat}K_{oc}f_{oc}^{coat}f_{avail}$)	14 nap 49 ace 210 phen	5.1	39

[a] Gt = goethite, K = kaolinite, Gb = gibbsite, Chlr = chlorite, M = mica, amFeOx = amorphous iron oxide.

estimates were much lower still, ranging from 3×10^{-16} to 7×10^{-19} $cm^2\ s^{-1}$. These results can be used in a mass transfer expression analogous to eq 1 to examine the hypothesis that intraorganic matter diffusion was rate limiting in our study of three HOCs with one sand. For this case, the sorption rate constant would be given by

$$k = \frac{D_{OM}}{\delta_{OM}^2}G \tag{6}$$

where D_{OM} is the HOC diffusivity within the OM, G again refers to any geometric or system factors, and δ_{OM} is the OM thickness. First, we note that the range in elastomer diffusivities given above (i.e., about 30) is consistent with our range of observed k_r values found for the three PAHs in the PB sand (range of about 20). As expected, if one assumes that natural OM is "glassy", the range of diffusivities (about 400) appears to be much too great to explain our data. Second, the diffusion path lengths, δ_{OM}, deduced by assuming the lower limit for $G = 1$ for the elastomer-like case, are found to be between 0.2 and 0.4 μm. If G is larger, then δ_{OM} must increase. While not out of the question (see ref 16), these OM thicknesses seem too large. Organic matter of this size should be observable by electron microscopy methods; we have not seen evidence for this. Furthermore, other workers have reported or implied OM thicknesses in natural solids to be on the order of tens of nanometers thick (*14, 15, 58*). These nanometer-scale thicknesses require diffusivities like those estimated for "glassy" polymers above. Thus, the intraorganic matter diffusion rate limitation seems to fail either because (a) the "best-fit" OM thicknesses appear to be unreasonably large (as for "elastomer" polymers) or (b) the variation in sorption rates as a function of HOC hydrophobicity is too great (as for "glassy" polymers).

Three Sands. Comparing the acenaphthene elution from the three different sand columns, one sees that the R_f value for GT is especially low considering that this column had a higher f_{oc} than the other sands (Table 2). This may indicate that not all of the GT organic matter was available for sorption. To some extent, all of the column K_d values deduced from the BTCs were lower than expected from predictions based on column f_{oc} and K_{oc} (PB by 50%, AJ by 75%, and GT by 95%). Furthermore, the column K_d values were less than those measured in batch tests [PB by 70%, AJ by 80%, and GT by 80% (*43*)]. To some degree, immobile water in the intact, coated sands should have *enhanced* the column K_d values relative to the potentially disaggregated sands used in batch testing. Thus, we believe that the HOCs being transported in the sand columns were not interacting with all of the OM present, even at flow rates comparable to those of groundwater flow.

When we compared the ratio of acenaphthene sorption rates observed in the three sand sorbents, we found a large discrepancy between the observed and predicted relative sorption rate ratios (Table 3). The second moment fits (Table 2) give relative k_r values of 1:0.4:0.55 for PB:GT:AJ. For GT and AJ, these are 30 and 3 times higher, respectively, than predicted from the coating model (ignoring any differences in the parameter G). Obviously, either we are not modeling the rate-limiting sorption step in each case or we have left some important factor out of the retarded diffusion model.

The high relative k_r values imply that observed diffusion rates are faster than we predict from the coating model. We believe that sand-to-sand variations in porosity, tortuosity, and constrictivity (i.e., factors combined into G) do not explain the discrepancy because (a) our measures of coating porosity do not differ widely and (b) constrictivity effects can be neglected when measured pore diameters (>3 nm quantified) are large relative to the size of the sorbates (~8 Å diameter). Our results could also be explained by errors in our estimates of the diffusion path lengths, δ. Lower δ values would dramatically increase the predicted sorption rate because of the squared dependence of k_r on path length. For GT, we calculate that a δ value of about 17 μm (rather than the value of 100 μm observed microscopically) would give the measured k_r ratio to PB. Similarly, reducing the average path length in AJ to about 11 μm (rather than 20 μm) brings the predicted ratio into agreement with the measured value. For AJ, this change in diffusion path length is reasonable (and only a factor of about 2); but for GT, the observed coating dimensions were clearly much larger than 17 μm (see Figure 1b). Thus, variations in the parameters G and δ are probably not the cause of the relative rates discrepancy for the three sands.

Unavailable Organic Matter in Intact Aquifer Sands. Another way to explain the discrepancy is to consider that we overestimated the retardation factor within the coatings (R_{coat}).

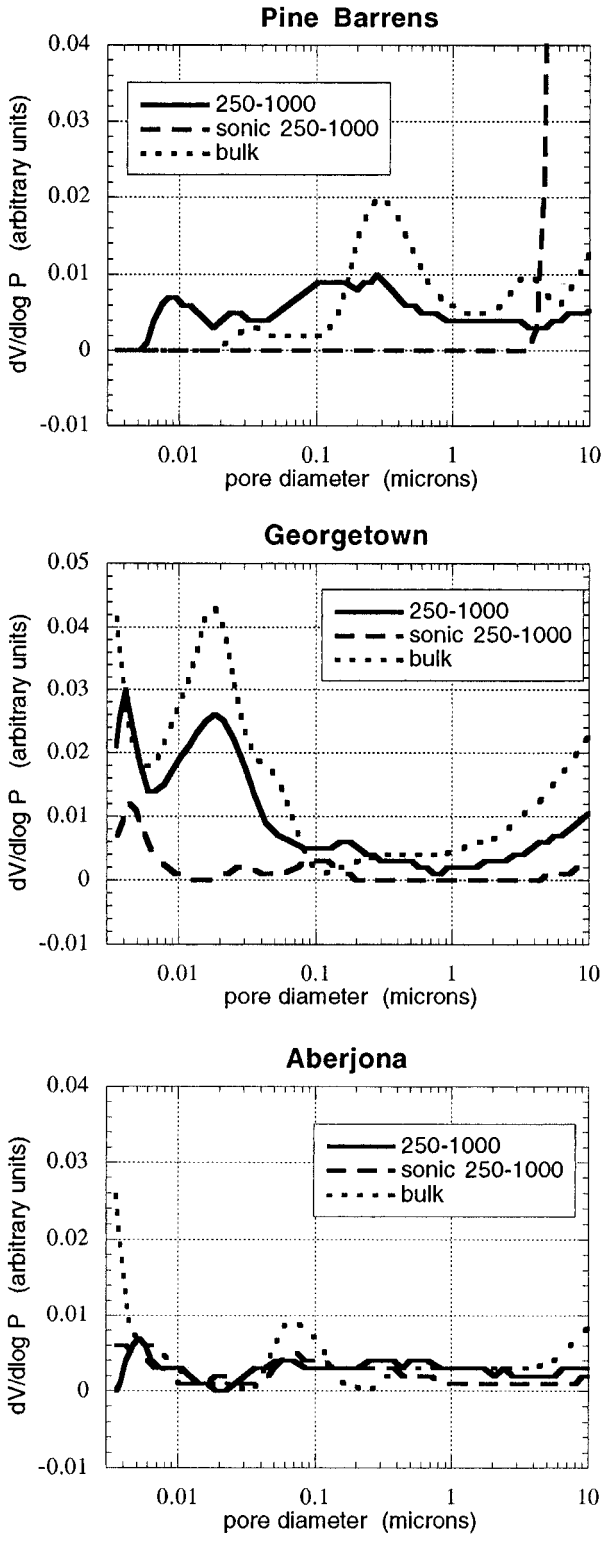

FIGURE 2. Mercury porosimetry data for three sorbents. For each sand, three subsamples were analyzed: 250−1000 μm, sonicated 250−1000 μm, and the bulk sand. The pore volume difference between sonicated and unsonicated 250−1000 μm samples over the pore diameter range 3−200 nm was used to calculate coating porosity, n_{coat}. The vertical axis (d *V*/d log *P*) represents the change in pore volume to change in log (applied pressure) during mercury intrusion.

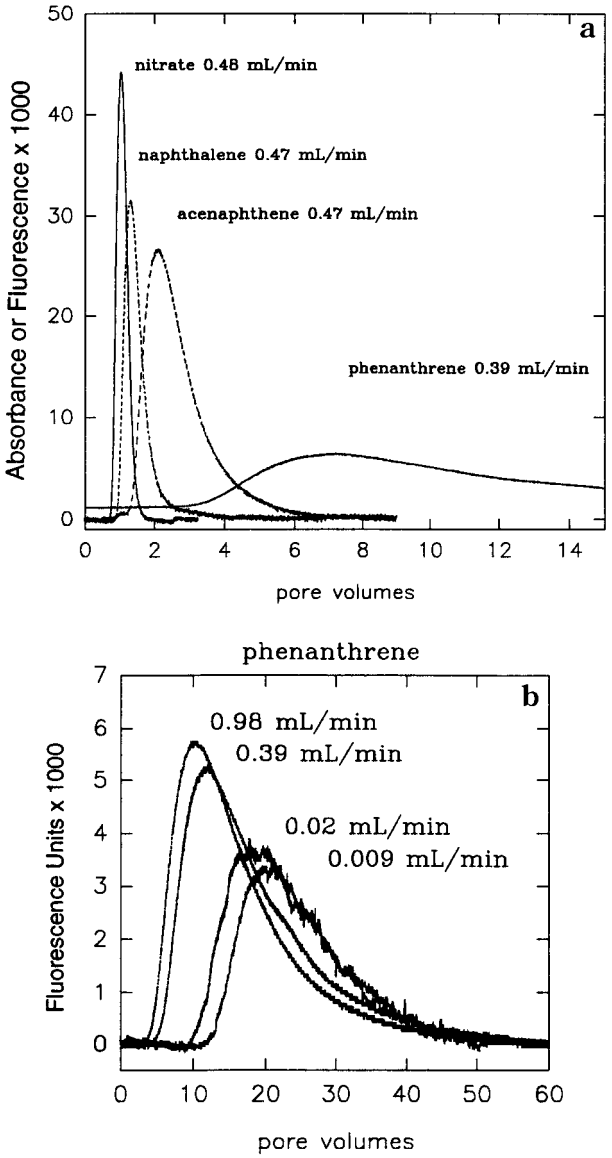

FIGURE 3. (a) Pine Barrens column elution curves for four compounds at flow rate of about 0.4 mL/min. Molar absorptivities (M^{-1} cm^{-1}) for the solutes are 1450 (nitrate), 4800 (nap), and 23 000 (ace). (b) Elution curves for phenanthrene/PB as a function of column flow rate. Phenanthrene fluorescence response for a 5.6 μM solution is 0.04 fluorescence units.

The K_d for the GT column (0.18 mL/g), calculated from R_f and column r_{sw}, was 20 times lower than the product, $K_{oc}f_{oc}$, for the bulk sand (3.7 mL/g). For PB, this ratio of column K_d to $K_{oc}f_{oc}$ is about 2 (0.82 vs 1.63), and for AJ it is a factor of 4 (0.59 vs 2.24). These differences could result from including measurable OM in our coating f_{oc} values, although such OM is not accessible to HOCs diffusing into the intact sand coatings. This "unavailable OM" hypothesis is also consistent with our observation that the column K_d values were always found to be much less than we measured in batch testing. Previously, Pignatello (*3*) suggested encasement of organic matter in the iron and aluminum oxyhydroxide minerals in soils. The possibility of encasement of organic matter in the oxyhydroxide minerals of the coatings is consistent with association of bacterial cells with ferrihydrite in sediments from acidic environments (*59*). It has also been reported that natural goethites contain up to 2 wt % carbon (*60*). If the surface association of organic anions with positively charged iron oxide mineral surfaces in many soils and sediments (*29, 30, 32−35, 61*) results in the inclusion of organic matter in diagenetically accumulating iron oxides, such OM may not be available later for HOC sorption. Thus, we suspect that overestimation of R_{coat} in the diffusion model, as applied to intact sands, is the most important cause of the lack of correspondence between the model and our moment results.

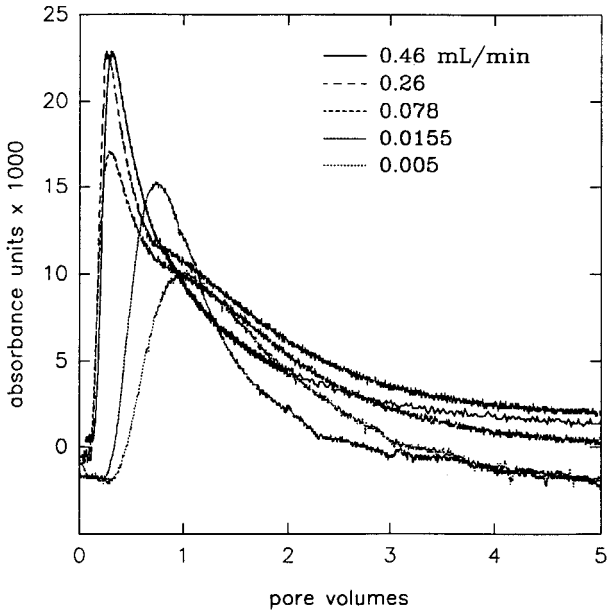

FIGURE 4. Georgetown–acetone elution curves at five flow rates indicating the asymmetric nature of the curves that reflect the presence of immobile water in this column.

TABLE 2. Column Experiment Variables and Deductions from Moment Fits

property	PB	GT	AJ
column f_{oc} (%)	0.048 (0.003)	0.109 (0.025)	0.066 (0.004)
column porosity	0.42	0.27	0.27
column r_{sw}	3.7	6.8	6.8
α (cm)[a]	0.05 ± 0.01 1.5 + 0.05 nap	0.56 ± 0.09	0.14 ± 0.01
R_f [b]	4.0 ± 0.14 ace 25 ± 0.5 phen 1.3 ± 0.3 nap	2.2 ± 0.15	4.8 ± 0.38
k_r (h^{-1})[c]	0.4 ± 0.15 ace 0.06 ± 0.03 phen	0.16 ± 0.06	0.22 ± 0.06

[a] From conservative tracer second moment fit. [b] From sorbate first moment fit. [c] From sorbate second moment fit.

If one accepts the premise that some portion of each sand's organic matter is completely unavailable for sorption, then R_{coat} in eq 1 can be modified to a coating retardation factor that incorporates the fraction of sorbent OM available for sorption:

$$R'_{coat} = 1 + r_{sw}^{coat} K_{oc} f_{oc}^{coat} f_{avail} \quad (7)$$

The fraction available (f_{avail}) can be estimated from the equilibrium behavior of the column (K_d deduced from μ'_1) versus expectations from $K_{oc}f_{oc}$. Thus we would expect R'_{coat} for the GT sand to be about 20 times lower than the value calculated from K_{oc} and coating f_{oc}. Making this adjustment to coating K_d for all three sands and acenaphthene, the values for coating retardation factor, R'_{coat}, become for GT, 5.1 instead of 83; for AJ, 39 instead of 150; and for PB, 49 instead of 97 (Table 1). Using these revised estimates of HOC interaction with coating OM, the relative sorption rates based on $[R'_{coat}\delta^2]^{-1}$ are 1:0.1:0.32 for PB:GT:AJ. These adjusted relative sorption rates agree within a factor of 4 with the observed ratios (Table 3), a very acceptable correspondence given our uncertainties in δ values.

This successful fitting suggests that, for coated aquifer materials, organic matter may be "buried" within the authigenically derived mineral phases that make up the coating sorption regime. Furthermore, the organic matter fraction

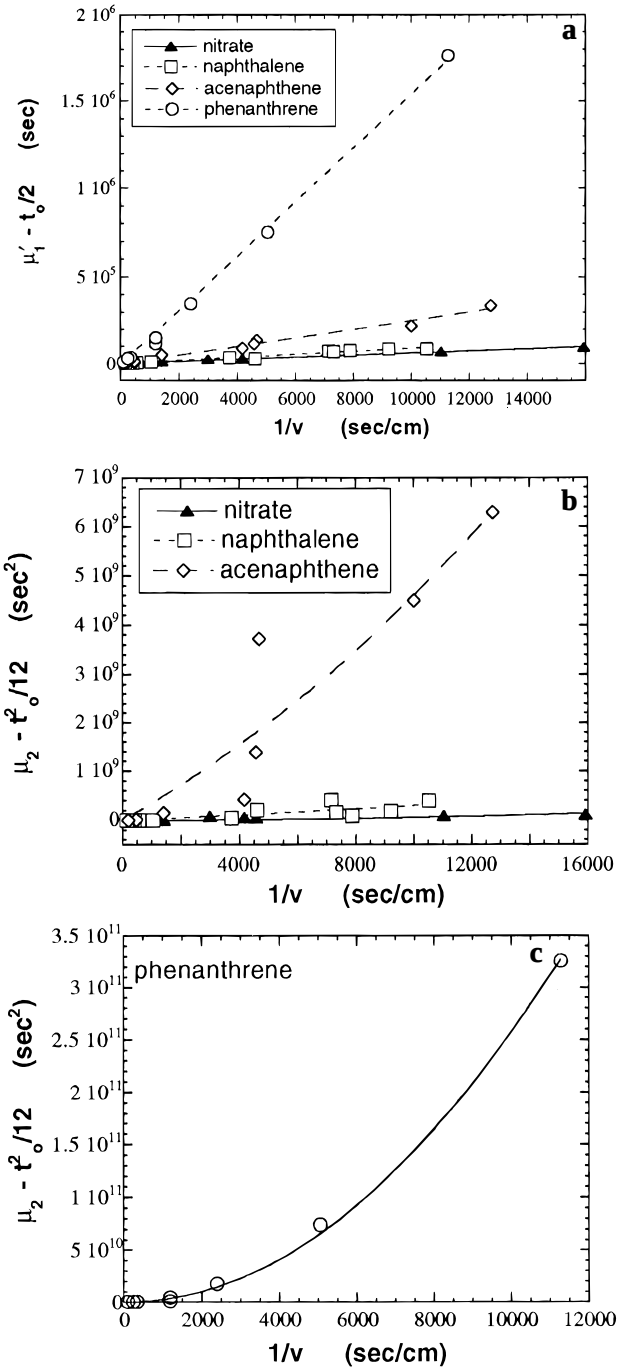

FIGURE 5. Moment plots and curve fits (lines) for Pine Barrens column data. (a) First moments versus inverse velocity. The slopes of these lines were used to calculate R_f values using eq 2. (b and c) Second moment data for four compounds were fit to eq 3 to quantify α and k_r.

available for sorption in the field may be much more accurately estimated from column K_d than calculated from $K_{oc}f_{oc}$ or even measured in batch test procedures with the same aquifer sands! We suspect that disaggregation of the solids, as in batch tests where suspensions are tumbled, may expose this organic matter. However, in column tests (and in the field!), the coatings remain intact and prevent all the organic matter from contributing to sorption. For solid matrices with abundant, evenly distributed organic matter (e.g., plankton debris in marine ooze), we would not expect batch-column discrepancies in K_d as observed for the aquifer sands we studied.

Semi-Empirical Estimation of HOC Sorption Rates to Aquifer Sands. Diffusion models, unlike first-order models,

TABLE 3. Relative Sorption Mass Transfer Coefficients: Predicted and Measured

	predicted	measured
3 HOCs/1 Sand		
	nap:ace:phen	nap:ace:phen
k_r proportional to $[R_{coat}]^{-1}$	3.5:1:0.23	3.3:1:0.15
3 Sands/1 HOC		
	PB:GT:AJ	PB:GT:AJ
k_r proportional to $[\delta^2 R_{coat}]^{-1}$	1:0.01:0.16	1:0.4:0.55
k_r proportional to $[\delta^2 R'_{coat}]^{-1}$ where R'_{coat} includes effect of f_{avail} factor	1:0.1:0.32	1:0.4:0.55

explicitly include parameters with physical meaning (e.g., diffusivity and path length). Such factors can potentially be estimated independently of sorption experimentation, and thus their application for particular HOC/sand combinations of interest may enable prediction of corresponding sorption rates.

For the three aquifer sands we studied, we propose that HOC sorption is rate-limited by retarded diffusion within the fine-grained iron oxide and aluminosilicate clay coatings on, and aggregate matrices between, primary mineral grains. For the sands and HOC sorbates we studied, measured first-order sorption rate constants ranged from about 0.1 to 1.0 h^{-1} (Table 2). Our analysis of these rate coefficients with the coating diffusion model above suggests the following general estimator for sorption rate in such aggregated sands:

$$k_r = \frac{D_{aq}}{\delta^2(1 + r_{sw}^{coat} K_{oc} f_{oc}^{coat} f_{avail})} G \qquad (8)$$

where G is a factor reflecting the following (a) characteristics of the system (i.e., r_{sw}, K_d, closed vs open system, particle shape) similar to that used by Wu and Gschwend (*20*) and Rao et al. (*41*); (b) the influence of porosity, constrictivity, and tortuosity factors of the microscale sorption regime as discussed by Ball and Roberts (*4*). Since the coating model appears to have successfully estimated *relative* sorption rates, it suggests that our approaches for obtaining sand and HOC properties to estimate $[R'_{coat}\delta^2]^{-1}$ were reasonable. Aqueous diffusivities can be readily calculated using expressions such as that of Hayduk and Laudie (*62*) based on sorbate molar volumes (cm^3/mol) and an assumed water viscosity (cP) at the temperature of interest.

Thus, the factor G remains as a fitting parameter for estimating the *absolute* k_r value for a given sorbate−sorbent pair. We evaluate G for our sorbent/HOC combinations by comparing the predicted k_r value derived from eq 8 with the k_r values deduced from our column breakthrough curves (Table 5). The ratio of k_r(measured) to k_r(predicted) gives the value of G for each case. The G values are very consistent for a given sorbent (PB) and the three sorbates (mean = 0.00064, σ = 0.000094), varying by less than 20% RSD (Table 5). For the three sand sorbents and acenaphthene, variation in G is somewhat greater: 0.0018 ± 0.0013. For all five sorbate−sorbent combinations we tested, the value of G was reasonably similar.

Considering the differences in composition, texture, and depositional/diagenetic history of these sorbents, the relatively narrow range in the values of the geometric correction factors, G, for the three sands suggests a semi-empirical estimator of sorption rates for HOCs on coated aquifer sands may be warranted. For sandy aquifer materials with iron oxide−aluminosilicate clay coatings, a G value of about 0.001 appears to give a sorption rate that is within a factor of a few of the "true" value. Geometric correction factors of this order of magnitude are comparable to the inverse of effective tortuosity values reported in the literature for other aquifer materials and nonpolar organic sorbates (*4, 5, 7, 63−65*). Hence, we suggest

$$k_r\ (h^{-1}) = \frac{0.001 D_{aq}}{\delta^2(1 + r_{sw}^{coat} K_{oc} f_{oc}^{coat} f_{avail})} \qquad (9)$$

This semi-empirical predictor should be useful for site characterization given careful description of the sorbent's microscale textural (δ, r_{sw}^{coat}) and chemical composition (f_{oc}^{coat}, f_{avail}). The diffusion model parameters are based on grain-scale phenomenon, thus the predicted rates should readily apply to sorption at the field scale. Furthermore, since eq 9 is based on the statistical averaging of experimental breakthrough curves over a range of sorbate−sorbent contact times, it should give a reasonable approximation of sorption kinetics under a wide range of field conditions.

Sorption Time Scales for HOCs in Coated Aquifer Sands. In order to assess the relative importance of sorptive exchange versus other subsurface processes, it is useful to contrast the time scales of the various competing processes of interest. Since the first-order model forward (k_f) and reverse (k_r) mass transfer rate constants (s^{-1}) must be related by

$$k_f = (K_d k_r) r_{sw} \qquad (10)$$

then HOC sorption to aquifer sands exhibits a time scale of

$$t_{sorption} = (k_f + k_r)^{-1} = [(K_d r_{sw} + 1) k_r]^{-1}$$

$$\approx \left[(K_d r_{sw} + 1)\frac{0.001 D_{aq}}{\delta^2 R'_{coat}}\right]^{-1} \qquad (11)$$

where K_d reflects only the available natural OM. For our sands and HOCs, such time scales ranged from 0.5 (nap/PB) to 3 (ace/GT) h. Since $R'_{coat} = 1 + r_{sw}K_d$, eq 11 is reasonably approximated by

$$t_{sorption} \approx \left[\frac{0.001 D_{aq}}{\delta^2}\right]^{-1} \qquad (12)$$

This result clearly identifies the importance of the diffusion

TABLE 4. Polymer Diffusion Model Parameters[a]

	elastomer			glassy		
	nap	ace	phen	nap	ace	phen
D_{OM} (cm^2/s)	1.5×10^{-12}	2.2×10^{-13}	3.1×10^{-14}	2.8×10^{-16}	1.5×10^{-17}	7.2×10^{-19}
δ_{OM} (μm)	0.40	0.20	0.18	7.8×10^{-5}	1.4×10^{-5}	4.3×10^{-6}
			nap:ace:phen		nap:ace:phen	
relative D_{OM}			6.6:1:0.14		18.4:1:0.05	

[a] D_{OM} based on model of Salame (*57*) using representative polymer parameters. δ_{OM} calculated from measured sorption rates, k_r, and D_{OM} using eq 6 and ignoring G.

TABLE 5. Measured and Predicted k_r Values and Geometric Correction Factors[a]

	PB	GT	AJ
predicted k_r (h^{-1}) (eq 8)	2010*G* nap 530*G* ace 120*G* phen	50*G*	170*G*
measured k_r (h^{-1})	1.3 nap 0.4 ace 0.06 phen	0.16	0.22
G = meas/predict	0.00065 nap 0.00075 ace 0.00052 phen	0.0032	0.0013

[a] Mean G for PB = 0.00064 ± 0.000094. Mean G for all HOCs and sands (n = 5) = 0.0018 ± 0.0013.

path length for controlling the times needed to approach sorptive equilibrium in aquifer solids of interest.

The time scales for exchange between solid and water in these sorbents (hours) are long enough that grain-scale desorption kinetics could be the limiting factor when groundwater contact times are short such as under pump-and-treat remediation conditions. The effect would be more pronounced for more hydrophobic organic compounds and for sands with thick coatings or matrix buildups.

Acknowledgments

This work was supported by NIEHS Grant 2 P30 ESO 2109-11.

Literature Cited

(1) Brusseau, M. L.; Larsen, T.; Christensen, T. H. *Water Resour. Res.* **1991**, *27*, 1137.
(2) Roberts, P. V.; Goltz, M. N.; Mackay, D. M. *Water Resour. Res.* **1986**, *22*, 2047.
(3) Pignatello, J. J. *Environ. Toxicol. Chem.* **1990**, *9*, 1117.
(4) Ball, W. P.; Roberts, P. V. *Environ. Sci. Technol.* **1991**, *25*, 1237.
(5) Harmon, T. C.; Semprini, L.; Roberts, P. V. *J. Environ. Eng.* **1992**, *118*, 666.
(6) Pignatello, J. J.; Ferrandino, F. J.; Huang, L. Q. *Environ. Sci. Technol.* **1993**, *27*, 1563.
(7) Farrell, J.; Reinhard, M. *Environ. Sci. Technol.* **1994**, *28*, 63.
(8) Rao, P. S. C.; Rolston, D. E.; Jessup, R. E.; Davidson, J. M. *Soil Sci. Soc. Am. J.* **1980**, *44*, 1139.
(9) Wu, S.-C.; Gschwend, P. M. *Environ. Sci. Technol.* **1986**, *20*, 717.
(10) Chiou, C. T.; Peters, L. J.; Freed, V. H. *Science* **1979**, *206*, 831.
(11) Karickhoff, S. W.; Brown, D. S.; Scott, T. A. *Water Res.* **1979**, *13*, 241.
(12) Schwarzenbach, R. P.; Westall, J. *Environ. Sci. Technol.* **1981**, *15*, 1360.
(13) Kopinke, F.-D.; Porschmann, J.; Stottmeister, U. *Environ. Sci. Technol.* **1995**, *29*, 941.
(14) Carroll, K. M.; Harkness, M. R.; Bracco, A. A.; Balcarcel, R. R. *Environ. Sci. Technol.* **1994**, *28*, 253.
(15) Carroll, K. M.; Harkness, M. R. *Environ. Sci. Technol.* **1995**, *29*, 285.
(16) Phillips, L. W.; Jafvert, C. T. *Environ. Sci. Technol.* **1995**, *29*, 283.
(17) Rogers, C. E. In *Physics and Chemistry of the Organic Solid State*; Fox, D., Labes, M. M., Weissberger, A., Eds.; Wiley Interscience: New York, 1965; Vol. II, p 509.
(18) Brusseau, M. L.; Rao, P. S. C. *Environ. Sci. Technol.* **1991**, *25*, 1501.
(19) Hutzler, N. J.; Crittenden, J. C.; Gierke, J. S. *Water Resour. Res.* **1986**, *22*, 285.
(20) Wu, S.-C.; Gschwend, P. M. *Water Resour. Res.* **1988**, *24*, 1373.
(21) Steinberg, S. M.; Pignatello, J. J.; Sawhney, B. L. *Environ. Sci. Technol.* **1987**, *21*, 1201.
(22) Stauffer, T. B. Ph.D. Thesis, College of William and Mary, 1987.
(23) MacIntyre, W. G.; Stauffer, T. B.; Antworth, C. P. *Ground Water* **1991**, *29*, 908.
(24) Ball, W. P.; Buehler, C. H.; Harmon, T. C.; Mackay, D. M.; Roberts, P. V. *J. Contam. Hydrol.* **1990**, *5*, 253.
(25) Wood, W. W.; Kraemer, T. F.; Hearn, J., P. P. *Science* **1990**, *247*, 1569.
(26) Ryan, J. N.; Gschwend, P. M. *Geochim. Cosmochim. Acta* **1992**, *56*, 1507.
(27) Barber, L. B., II; Thurman, E. M.; Runnells, D. D. *J. Contam. Hydrol.* **1992**, *9*, 35.
(28) Davis, J. A. *Geochim. Cosmochim. Acta* **1982**, *46*, 2381.
(29) Tipping, E. *Geochim. Cosmochim. Acta* **1981**, *45*, 191.
(30) Schnitzer, M.; Kodama, H. *Soil Sci. Soc. Am. J.* **1992**, *56*, 1099.
(31) Jardine, P. M.; Weber, N. L.; McCarthy, J. F. *Soil Sci. Soc. Am. J.* **1989**, *53*, 1378.
(32) Fontes, M. R.; Weed, S. B.; Bowen, L. H. *Soil Sci. Soc. Am. J.* **1992**, *56*, 982.
(33) Schwertmann, U. *Nature* **1966**, *21*, 645.
(34) Schwertmann, U.; Fischer, W. R.; Papendorf, H. *9th International Congress of Soil Science*, Adelaide, Australia, 1968; American Elsevier Publishing Company, Inc.: New York, 1968; p 645.
(35) Cornell, R. M.; Schwertmann, U. *Clays Clay Miner.* **1979**, *27*, 402.
(36) Karickhoff, S. W. In *Contaminants and Sediments*; Baker, R. A., Ed.; Ann Arbor Science: Ann Arbor, MI, 1980; Vol. 2, p 193.
(37) Karickhoff, S. W. *J. Hydr. Eng.* **1984**, *110*, 707.
(38) Chiou, C. T.; Porter, P. E.; Schmedding, D. W. *Environ. Sci. Technol.* **1983**, *17*, 227.
(39) Schneider, P. *Chem. Eng. Sci.* **1986**, *41*, 1759.
(40) Parker, J. C.; Valocchi, A. J. *Water Resour. Res.* **1986**, *22*, 399.
(41) Rao, P. S. C.; Jessup, R. E.; Rolston, D. E.; Davidson, J. M.; Kilcrease, D. P. *Soil Sci. Soc. Am. J.* **1980**, *44*, 684.
(42) Lowell, S.; Shields, J. E. In *Powder Surface Area and Porosity*; Chapman & Hall: London, 1984, p 97.
(43) Holmén, B. A. Ph.D. Thesis, Massachusetts Institute of Technology, 1995.
(44) Ryan, J. N.; Gschwend, P. M. *Clays Clay Miner.* **1991**, *39*, 509.
(45) Jackson, M. L.; Lim, C. H.; Zelazny, L. W. In *Methods of Soil Analysis. Part 1, Physical and Mineralogical Methods*; Klute, A., Ed.; American Society of Agronomy, Inc.: Madison, WI, 1986; p 101.
(46) Miller, M. M.; Wasik, S. P.; Huang, G.-L.; Shiu, W.-Y.; Mackay, D. *Environ. Sci. Technol.* **1985**, *19*, 522.
(47) Karickhoff, S. W. *Chemosphere* **1981**, *10*, 833.
(48) Valocchi, A. J. *Water Resour. Res.* **1985**, *21*, 808.
(49) Parker, J. C.; van Genuchten, M. T. *Determining transport parameters from laboratory and field tracer experiments*; Bulletin 84-3; Virginia Agricultural Experimental Station: Leesburg, VA, 1984.
(50) Freeze, R. A.; Cherry, J. A. *Groundwater*; Prentice-Hall, Inc.: Englewood Cliffs, NJ, 1979.
(51) Lee, L. S.; Rao, P. S. C.; Brusseau, M. L.; Ogwada, R. A. *Environ. Toxicol. Chem.* **1988**, *7*, 779.
(52) Brusseau, M. L. *Water Resour. Res.* **1993**, *29*, 1071.
(53) Roberts, P. V.; Goltz, M. N.; Summers, R. S.; Crittenden, J. C.; Nkedi-Kizza, P. *J. Contam. Hydrol.* **1987**, *1*, 375.
(54) Han, N.; Bhakta, J.; Carbonell, R. G. *AIChE J.* **1985**, *31*, 277.
(55) Carbonell, R. G. *Chem. Eng. Sci.* **1979**, *34*, 1031.
(56) Freeman, D. H.; Cheung, L. S. *Science* **1981**, *214*, 790.
(57) Salame, M. *Polym. Eng. Sci.* **1986**, *26*, 1543.
(58) Mayer, L. M. *Geochim. Cosmochim. Acta* **1994**, *58*, 1271.
(59) Ferris, F. G.; Tazaki, K.; Fyfe, W. S. *Chem. Geol.* **1988**, *74*, 321.
(60) Yapp, C. J.; Poths, H. *Geochim. Cosmochim. Acta* **1986**, *50*, 1213.
(61) Wang, H. D.; White, G. N.; Turner, F. T.; Dixon, J. B. *Soil Sci. Soc. Am. J.* **1993**, *57*, 1381.
(62) Hayduk, W.; Laudie, H. *AIChE J.* **1974**, *20*, 611.
(63) Harmon, T. C.; Roberts, P. V. *Environ. Sci. Technol.* **1994**, *28*, 1650.
(64) Grathwohl, P.; Reinhard, M. *Environ. Sci. Technol.* **1993**, *27*, 2360.
(65) Pedit, J. A.; Miller, C. T. *Environ. Sci. Technol.* **1995**, *29*, 1766.

Received for review February 22, 1996. Revised manuscript received August 28, 1996. Accepted September 3, 1996.[⊗]

ES9601696

[⊗] Abstract published in *Advance ACS Abstracts,* November 15, 1996.